Rare Metal Materials and Engineering
Volume 55, Issue 8, August 2026
Available online at www.rmme.ac.cn

Science Press

Cite this article as: Geng Chuanwen, Zhao Peng, Su Yi, et al. Effect of H_2 on 8YSZ Coatings Prepared by Arc Plasma Torch[J]. Rare Metal Materials and Engineering, 2026, 55(08): 1858-1864. DOI: https://doi.org/10.12442/j.issn.1002-185X.20250436.

ARTICLE

Effect of H_2 on 8YSZ Coatings Prepared by Arc Plasma Torch

Geng Chuanwen[1], Zhao Peng[2], Su Yi[2], Fan Zihao[3], Wu Xi[4]

[1] School of Carbon Neutrality Science and Engineering, Anhui University of Science & Technology, Hefei 232001, China; [2] Institute of Plasma Physics, Chinese Academy of Sciences, Hefei 230031, China; [3] School of Metallurgical Engineering, Anhui University of Technology, Ma'anshan 243032, China; [4] College of Chemistry and Chemical Engineering, Shihezi University, Shihezi 832003, China

Abstract: The thermal barrier coatings (TBCs) are prepared using spraying technique of 8YSZ particles. In this process, H_2 is often added to the plasma torch discharge system. In order to study the effect of H_2 content on plasma discharge, this study emplyed particle velocity capture diagnostics, optical emission spectroscopy, and finite element simulation to validate the relationship between H_2 content and coating quality. The results indicate that adding H_2 increases the temperature and velocity of plasma, which in turn improves the efficiency and in-flight velocity of molten 8YSZ particles. However, when the $H_2/(Ar+H_2)$ is increased to 50%, the instability of arc root disturbs the arc plasma discharge, posing a challenge to maintaining the physical state of the in-flight particles. With an increase in H_2 flow rate, the coating quality shows a trend of first increasing and then decreasing, with the optimal flow rate ratio being $H_2/(Ar+H_2)$= 37.5%. The findings of this work can serve as a theoretical guidance and reference for the preparation of TBCs via plasma.

Key words: in-flight particles; 8YSZ coatings; plasma torch; H_2 plasma

1 Introduction

The service environment of hot-end components is getting harsher as the front temperature of aero-engine turbine rises. The base metal temperature reaches 1000 °C or higher, surpassing the service limit of nickel-based superalloys due to high-temperature oxidation and gas flow erosion[1–2]. Thermal barrier coatings (TBCs), which can offer thermal insulation as well as oxidation and corrosion resistance, are indispensable for protecting substrate materials, thereby enabling hot-end components to operate at elevated temperatures[3–4]. Physicochemical properties, such as high refractoriness, chemical inertness, phase stability, low thermal conductivity, low density, and high thermal reflectivity, are essential for TBCs[5–7]. Due to its low thermal conductivity (λ<2.5 $W\cdot m^{-1}\cdot K^{-1}$), high fracture toughness (Γ =210 J/m^2), and well-matched coefficient of thermal expansion (α=10.8×10^{-6} K^{-1}, $\alpha_{substrate}$=16×10^{-6} K^{-1}), 8mol% yttria-partially stabilized zirconia (8YSZ) exhibits excellent compatibility with the alloy matrix[8–11].

The most popular material for TBCs nowadays is 8YSZ. And one of the most crucial techniques for producing high-quality TBCs is plasma spraying. The main component of the plasma generator is a plasma torch, which produces a hot plasma that melts or semi-melts the sprayed material[12–14]. The molten droplets are sprayed quickly onto the surface of the pre-treated substrate, in which they are cooled and cured to form TBCs[15]. Over recent years, significant advancements have been achieved in spraying techniques and the performance of 8YSZ-based TBCs fabricated by plasma spraying. In order to form TBCs, Shi et al[16] exposed 8YSZ with varying size characteristics to atmospheric plasma spraying (APS). Results showed that the ceramic coatings made of nanostructured 8YSZ show reduced brittle fracture, low thermal diffusivity, and low conductivity. The effect of particle flight behavior on the microstructure and fracture toughness was studied by Xiao et al[17]. TBCs exhibit a denser microstructure, fewer structural defects, and superior fracture toughness when the in-flight temperature and velocity of 8YSZ are increased during plasma spraying. Xie et al[18] used low-pressure suspension plasma spraying to investigate the deposition mechanisms of coatings under inert and oxidizing atmospheres, and successfully fabricated high-density

Received date: August 20, 2025
Foundation item: Anhui University of Science and Technology (AUST) Introduction of Talents Start-up Fund (2024yjrc136); 2023 Anhui Major Industrial Innovation Plan Project in the field of Green and Low-Carbon (AHZDCYCX-LSDT2023-01)
Corresponding author: Geng Chuanwen, Ph. D., School of Carbon Neutrality Science and Engineering, Anhui University of Science & Technology, Hefei 232001, P. R. China, E-mail: chuanwen.geng@aust.edu.cn

nanostructured 8YSZ coatings via this strategy. Incorporating various oxides into 8YSZ can effectively suppress coating peeling and increase the thermal cycle life of plasma-sprayed TBCs[19–21].

The service life of TBCs is directly influenced by the heating level of the plasma torch on 8YSZ, which is a crucial component of plasma spraying technique. As the primary working gas of the plasma torch, argon (Ar) is a monoatomic noble gas with a low arc voltage, which is easier to discharge from a plasma torch than other gases and does not react with the deposited coatings[22]. Owing to its high enthalpy, adding a small amount of hydrogen (H_2) to argon can effectively increase the plasma temperature, elongate the flame length, prolong the residence time of 8YSZ particles, and promote more thorough melting of the feedstock[23–24]. Nevertheless, H_2 is currently employed as a reducing gas, which impacts flame flow state, in-flight particle, and plasma arc stability, ultimately leading to coating failure. In this study, the particle flight behavior was investigated by adjusting the H_2 content during APS, combined with finite element simulation of the plasma-powder heating process using ANSYS Fluent. The influence of H_2 content on plasma discharge characteristics and the quality of as-sprayed 8YSZ coatings was studied.

2 Experiment

Fig. 1 illustrates the preparation process of 8YSZ coatings using a physical diagnostic system. The apparatus used in this experiment was the SG-100 plasma torch (Praxair S. T. USA), which can generate a stable, controllable, and high-temperature with high-velocity compressed plasma arc[25]. The plasma torch was used for arc plasma discharge. The substrate material used in this experiment was stainless steel 316L. The

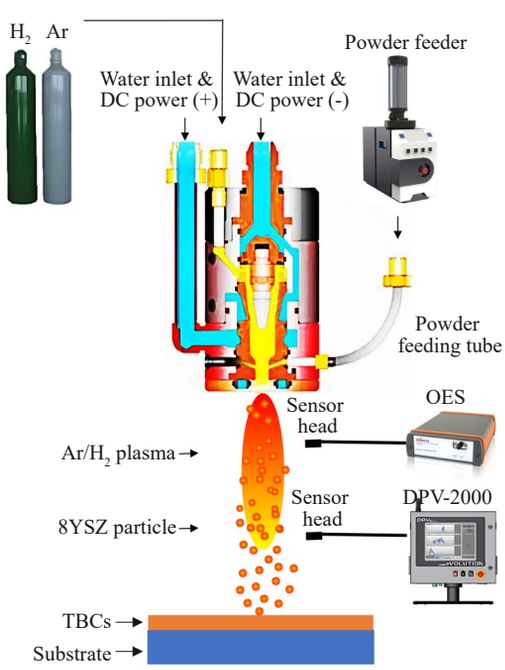

Fig.1 Schematic diagram of preparation process of 8YSZ coatings by plasma spraying

discharge power of plasma torch was 50 kW. The working gas flow rate was set to 40 L/min, with a powder feeding rate of 2 g/min. By increasing the H_2 content in the working gas, the effect of H_2 plasma on the sprayed 8YSZ was studied. Table 1 displays the flow rate ratio of discharge gas, with $H_2/(Ar+H_2)$ rising from 0% to 50%. The surface morphology and cross-sectional microstructure of the coatings were characterized using scanning electron microscope (SEM, ZEISS Sigma 300). The phase composition of the 8YSZ coatings was analyzed by X-ray diffractometer (XRD, Bruker D8 Advance).

Using the commercial computational fluid dynamics program ANSYS Fluent, a visual finite element simulation of plasma heating process of powder flow was conducted. The net energy (Q_n) of the in-flight 8YSZ particles is determined by the difference between the heat absorbed from the plasma by conduction and convection (Q_{cv}) and the heat dissipated from particle surface to the surroundings by radiation (Q_{prad}), as follows[26–27]:

$$Q_n = Q_{cv} - Q_{prad} \quad (1)$$

$$Q_{cv} = Ah_c\left(T_\infty - T_p\right) \quad (2)$$

$$Q_{prad} = A\varepsilon_p\sigma_{sb}\left(T_\infty^4 - T_p^4\right) \quad (3)$$

where A is surface area of particle; T_∞ is plasma temperature; T_p is particle temperature; σ_{sb} is Boltzmann constant; ε_p is emissivity; h_c is heat transfer coefficient.

Optical emission spectroscope (OES, AvaSpec) was used to analyze the effect of H_2 content variations on the discharge performance of plasma. The principle is that when atoms in the plasma are excited to a high energy level and then jump back to a lower energy level, they emit light with particular wavelength. By tracking the intensity and wavelength of the spectral lines, the composition and content of the plasma can be determined[28]. Based on the principles of infrared thermometry and double-slit photodiagnostics, the diagnostic apparatus DPV-EVOLUTION (DPV-2000) was employed to measure the temperature, velocity, and size of in-flight 8YSZ particles, which revealed the energy evolution behavior of particles under plasma action[29].

3 Results and Discussion

3.1 Microstructure and porosity

Fig.2 displays SEM images of original powder and coatings 1 – 5. The original powder is almost spherical in shape, as depicted in Fig. 2a, with the majority of the particle sizes falling between 30 and 50 μm. The surface of coating 1 exhibits spherical-like morphology, which is probably 8YSZ

Table 1 $H_2/(Ar+H_2)$ flow rate ratios

Coating	Flow rate of Ar/L·min^{-1}	Flow rate of H_2/L·min^{-1}	$H_2/(Ar+H_2)$
1	40	0	0%
2	35	5	12.5%
3	30	10	25.0%
4	25	15	37.5%
5	20	20	50.0%

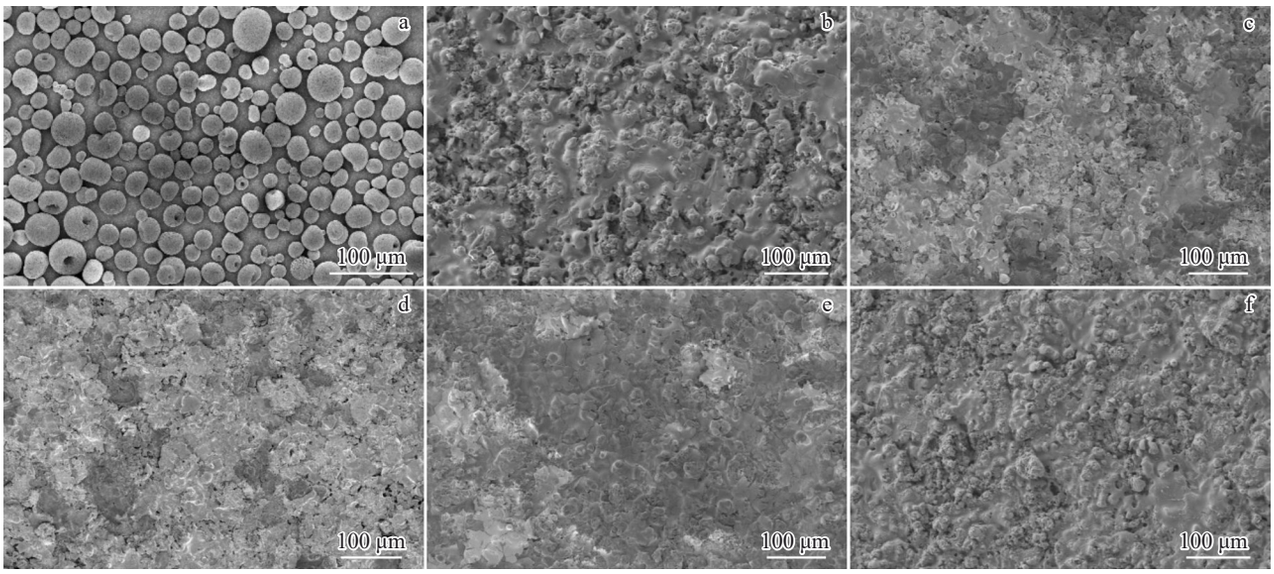

Fig.2 SEM images of the 8YSZ original powder (a) and different coatings (b–f): (b) coating 1, (c) coating 2, (d) coating 3, (e) coating 4, and (f) coating 5

particles that have not yet fully dissolved. Too many undissolved particles will cause excessively high porosity of the coating. Fig. 3 shows the cross-sectional porosity of different 8YSZ coatings. The cross-sectional porosity of coating 1 is 15.177%. Compared with coating 1, coating 2 shows smaller particle diameter. This suggests that addition of H_2 increases plasma temperature, which in turn heats the powder particles as they impact the substrate surface, thereby forming a denser coating. Additionally, the porosity of coating 2 decreases to 6.719%. In coating 3 and coating 4, the content of H_2 in working gas increases, resulting in less undissolved particles. The porosity of coating 3 and coating 4 is 5.084% and 3.411%, respectively. In addition, it can be seen that the surface of coating 4 is flatter than that of coating 3, and the corrosion resistance of coating 4 may be attributed to enhanced flatness and reduced porosity. In contrast, the coating surface shows more undissolved particles in coating 5 when H_2 content of working gas increases to 50.0%. This results in a significant increase in surface roughness, and the porosity rises to 8.392%. This may be related to high proportion of H_2-doped discharge, which causes discharge instability.

XRD patterns of original 8YSZ powders and coatings 1–5 are shown in Fig.4. The coatings 1–5 at the sprayed state are primarily composed of t phase (ZrO_2, non-equilibrium tetragonal phase). The overall m phase is reduced, indicating the better melting degree of the 8YSZ powders. In contrast, the 8YSZ powders are primarily composed of t phase with a small amount of m phase. The overall m phase content of the sprayed coating is lower than that of the 8YSZ powder, suggesting the higher melting point of the coatings 1 – 5. Nevertheless, XRD patterns of coatings 1, 2, and 5 show m phase peaks in the 2θ range of 25° – 29.5° , suggesting incomplete melting of the powder, which is also consistent with Fig. 2. During plasma spraying, the molten ceramic droplets undergo rapid cooling and solidification, yielding a non-equilibrium 8YSZ structure mainly composed of the non-transformable tetragonal phase (t') with a high Y_2O_3 content. The as-sprayed coating is predominantly composed of the t'

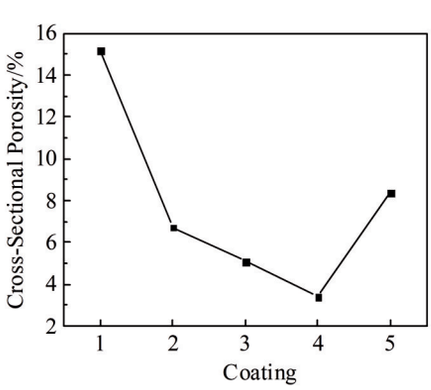

Fig.3 Cross-sectional porosity of different 8YSZ coatings

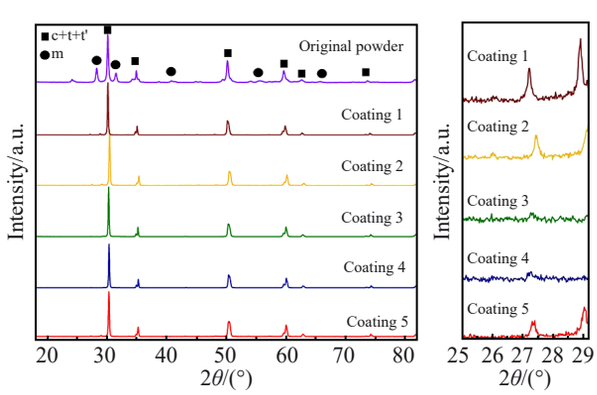

Fig.4 XRD patterns of 8YSZ original powder and coatings 1–5

phase, whereas a small amount of monoclinic m phase remains in the partially melted ceramic regions.

3.2 Finite element simulation

The finite element simulation of the reaction process of coatings 1–5 is shown in Fig. 5, which illustrates that adding H_2 to the plasma working gas progressively elevates the plasma temperature and flow velocity, thereby promoting the melting of high-melting-point 8YSZ for TBCs fabrication. H_2 shows the highest thermal conductivity and enthalpy. At standard atmospheric pressure and 15 000 K, the enthalpy of H_2 is 1.26×10^9 J/kg, while the enthalpy of Ar is 3.53×10^7 J/kg. At this temperature, the former is nearly 36 times greater than the latter. The H_2-rich hot plasma will significantly improve the thermal conductivity of arc, convective heat transfer between the gas and the arc, and the arc energy by increasing the H_2 content in the gas mixture[30]. The elongation of the jet length and the sharp increase in the plasma jet temperature and flow velocity at the nozzle demonstrate that, even with the plasma torch nozzle size remaining constant, the arc energy is significantly increased, and the collision between atoms and ions becomes more intense.

However, the plasma temperature and flow velocity decreases when the $H_2/(Ar+H_2)$ ratio is 50%. This is because the excessively high H_2 flow rate leads to a significant expansion of the flow field from the nozzle mouth to the jet tail, generating numerous eddies in the tail plume region of the plasma torch. These eddies make the plasma torch flame highly unstable in the tail plume region. And the heat escapes into the air due to these eddies, leading to systematic energy loss and low efficiency.

By altering the plasma temperature and flow velocity, the variation in the H_2 content also has an indirect impact on the temperature evolution of 8YSZ particles during flight. 8YSZ particles are normally melted at temperatures between approximately 2873.15 and 2973.15 K. Fig. 6 presents the finite element simulation results of 300 in-flight particles in the plasma, showing the spatial and quantitative distributions of particle temperature. Fig. 6a shows the heating history of powder for coatings 1–5. It is clear that the particles barely reach their melting point in the absence of H_2. This is consistent with the result of coating 1 in Fig. 6b, where the semi-molten particles increase the roughness of coatings. Particularly, it is evident that the particle temperature of coating 4 nearly reaches the melting point (Fig. 6b), and particle temperatures in coatings 2 – 4 show a successive increase. Semi-molten and fully molten particles can facilitate the preparation of coatings with high bonding strength, excellent flatness, and low porosity. The plasma discharge in coating 5 results in a decrease in particle temperature.

In order to study the interaction between 8YSZ particles and the plasma, OES was used to detect the plasma luminescence spectrum between 300 and 1000 nm, as shown in Fig. 7. The amount of powder evaporation can be represented visually by the intensity of the spectral emission. The measured data include Ar (690–900 nm), H_α (656.3 nm), and 8YSZ (300–500 nm).

To characterize the sprayed plasma, which governs the reaction processes between electron and particle within it, the electron excitation temperature must be calculated from OES

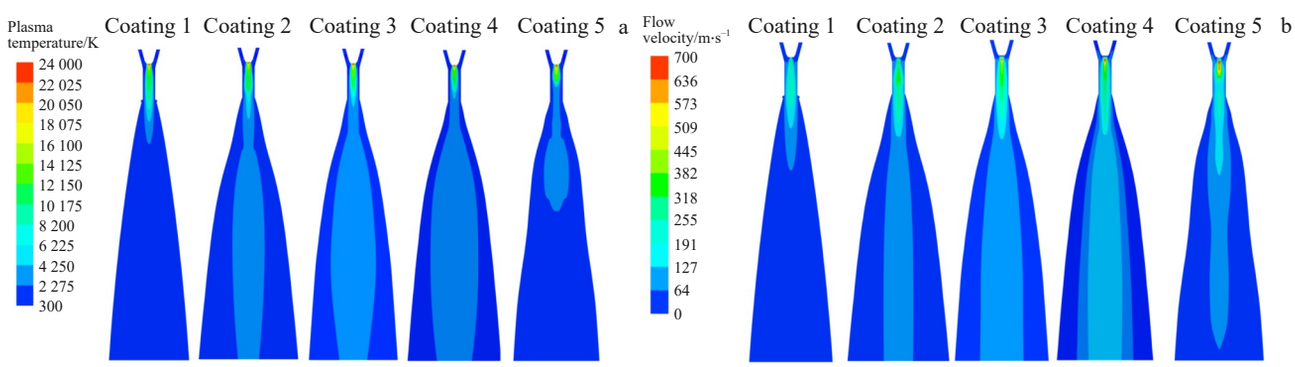

Fig.5 Finite element simulation results of coatings 1–5: (a) plasma temperature; (b) flow velocity

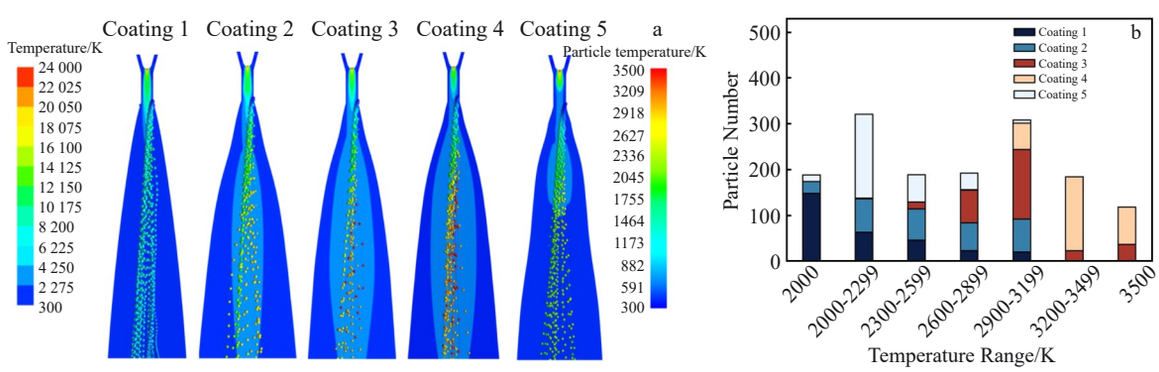

Fig.6 Finite element simulation results of spatial (a) and quantitative (b) distributions of particle temperature

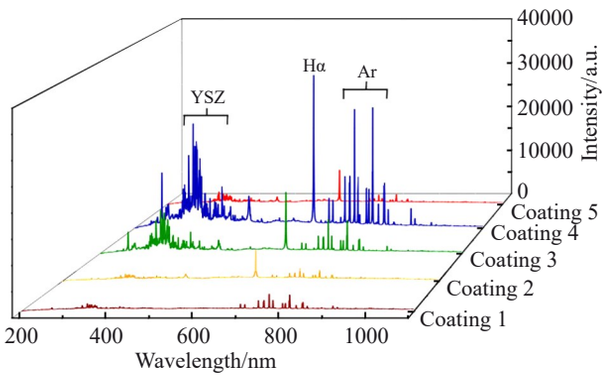

Fig.7 OES diagram of plasma flame flow of coatings 1–5

measurements. The Boltzmann slope method can be used to define the electronic excitation temperature (T_e) of plasma[31–32]. The specific calculation is as follows:

$$\ln\left(\frac{I_{ki}\lambda_{ki}}{g_k A_{ki}}\right) = \ln K - \frac{E_k}{k_B T_e} \quad (4)$$

where I_{ki} is spectral line radiation intensity; λ_{ki} is wavelength; g_k is statistical mass; A_{ki} is leaping chance; E_k is excitation energy; k_B is Boltzmann constant; K is constant.

Table 2 displays Ar I spectral lines and transition parameters selected for calculating T_e. All spectral data were acquired from National Institute of Standards and Technology.

The observed luminescence spectra of coatings 1 – 5 are displayed in Fig.7, and the Boltzmann fitting plots of a subset of the Ar I spectral lines from Fig. 7 are shown in Fig. 8. Compared with other coatings, the Ar I spectral line of coating 1 has a lower height, where H_2 is absent. Additionally, the spectral database shows that the 8YSZ powder has partially evaporated, as indicated by the spectral line appearing at 300 – 500 nm, and the fitting Boltzmann slope gives an electronic excitation temperature of 8351.06 K. When a tiny amount of H_2 is added (coating 2), a noticeable H_α (656.3 nm) appears, and the electronic excitation temperature rises to 9450.91 K. In contrast to coating 1, the 8YSZ spectral line of coating 2 shows no notable enhancement, due to the small H_2 addition that cannot sufficiently heat the powder. The Ar, H_α, and 8YSZ spectral lines of coatings 3 and 4 show a significant gradient increase with the increase in H_2 content, suggesting that H_2 significantly increases the energy of arc, convective heat transfer between the gas and the arc, and the thermal conductivity of arc. The electron excitation temperatures of coatings 3 and 4 reach 10 187.03 and 11 311.21 K, respectively. The substantial increase in arc energy is demonstrated by the increase in both jet length and temperature when nozzle remains constant in size. The high-temperature jet molecules collide with the powder particles as the 8YSZ powder passes through the plasma jet. This drastically alters the particle motion and heat transfer properties through the transfer of jet mass, momentum, and energy. Finally, coating 5 shows a spectral decrease as H_2 content increases further, and the electronic excitation temperature drops to 9611.14 K, which is consistent with coating 2 and matches the finite element simulation results in Fig.5.

Table 2 Ar I spectral lines and transition parameters selected for calculating T_e

λ/nm	$gA/\times10^7$ s^{-1}	E/eV
418.19	1.68	14.69
426.63	1.56	14.53
545.17	2.35	15.1
557.24	4.62	15.32
696.54	1.92	13.33
738.40	4.25	13.30
750.39	4.50	13.48
751.46	4.00	13.27
763.51	12.20	13.17
810.37	7.50	13.15

When the DPV-2000 probe was positioned 10 cm away from the plasma torch exit, the instrument automatically recorded the particle flight velocity. The particle flight velocity distribution of coatings 1 – 5 is displayed in Fig. 9, with the average flight velocities of 130, 102, 142, 158, and 117 m/s, respectively. The flight velocity distribution of Ar discharge particles alone is shown in the result of coating 1, and it is evident that fewer particles are captured, and the velocity distribution is not uniform. This is mainly attributed to the low temperature and velocity of the plasma jet, the failure to accelerate particles to the monitoring position, and the non-uniform heating of the particles. The uneven velocity distribution results in numerous irregular velocity profiles and relatively few smooth distributions. This gives rise to a non-centralized velocity distribution, which leads to a large number of rough surface features and only a small number of smooth surface regions, as illustrated in Fig.2b.

The particle flight velocity distributions in coatings 2 – 4 exhibit a concentrated trend, and the average velocity increases steadily with the increase in H_2 content. This phenomenon is attributed to the increased H_2 content in the working gas, which can effectively increase the temperature and flow velocity of the plasma. The high-energy plasma can more effectively transmit energy to the particles through momentum transfer process and thermal conduction, which eventually helps to optimize the particle motion velocity.

Interestingly, the average particle velocity of coating 1 is higher than that of coating 2. This is because fewer particles of coating 1 can reach the monitoring region, resulting in a significantly lower particle collision frequency than that of coating 2. Moreover, the higher plasma energy transfer efficiency of coating 2 increases the initial kinetic energy of the particles, thereby promoting particle collisions. As a result, part of the kinetic energy is dissipated as heat, leading to a lower average velocity of coating 2.

Furthermore, compared to coating 4, more unmelted particles in coating 3 are observed. This is attributed to the higher plasma heating intensity of particles in coating 4 caused by further increased H_2 content. As more particles are

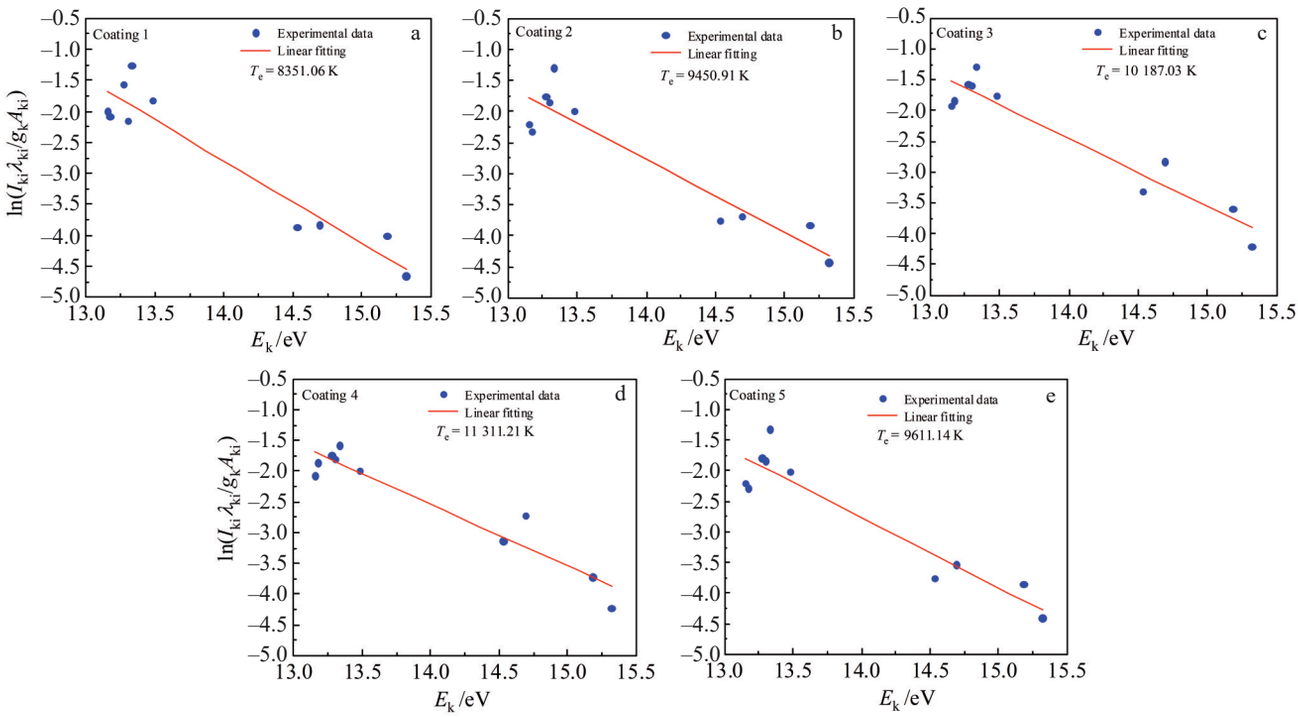

Fig.8 Boltzmann fitting plots of plasma electron excitation temperature of different coatings: (a) coating 1, (b) coating 2, (c) coating 3, (d) coating 4, and (e) coating 5

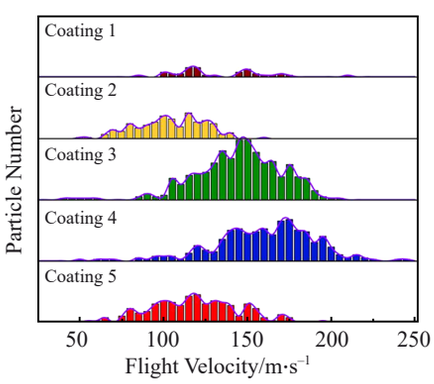

Fig.9 Flight velocity distribution of 8YSZ particles of coatings 1–5

evaporated upon reaching their evaporation point, the total number of detectable particles is decreased. As seen in Fig. 5, unstable plasma discharge occurs in coating 5 when the H_2 content is further increased. The disordered discharge process directly leads to a simultaneous decrease in both plasma temperature and flow velocity. The energy transferred from the plasma to the particles is significantly reduced, which ultimately manifested as a noticeable decrease in particle velocity. Therefore, the ideal flow rate ratio of the plasma torch working gas for creating high-quality 8YSZ coatings is $H_2/(Ar+H_2)$=37.5%.

4 Conclusions

1) Although increasing the H_2 content in the plasma torch working gas accelerates the melting of 8YSZ particles, improves the coating flatness, and reduces the porosity of coatings, an excessively high H_2 content of 50% actually deteriorates quality of the 8YSZ coating.

2) Using particle velocity capture diagnostics, OES, and finite element simulation, it was found that the increase in H_2 content can simultaneously improve plasma velocity and temperature, which in turn increases the efficiency and flight velocity of the molten 8YSZ particles. However, increasing H_2 content to 50% causes instability in the plasma arc, making it challenging to maintain physical state of the in-flight particles. Therefore, the ideal flow rate ratio of the plasma torch working gas for creating high-quality 8YSZ coatings is $H_2/(Ar+H_2)$=37.5%.

References

1 Iqbal A, Moskal G, Cavaleiro A *et al*. *Alexandria Engineering Journal*[J], 2024, 91: 161

2 Chen L, Li B H, Feng J. *Progress in Materials Science*[J], 2024, 144: 101265

3 Wei Z Y, Meng G H, Chen L *et al*. *Journal of Advanced Ceramics*[J], 2022, 11(7): 985

4 Jiang C R, Chen J, Zhu Z. *Ceramics International*[J], 2022, 48(9): 12271

5 Padture N P, Gell M, Jordan E H. *Science*[J], 2002, 296(5566): 280

6 Bakan E, Vaßen R. *Journal of Thermal Spray Technology*[J], 2017, 26(6): 992

7 Thakare J G, Pandey C, Mahapatra M M *et al*. *Metals and Materials International*[J], 2021, 27(7): 1947

8 Ren X R, Pan W. *Acta Materialia*[J], 2014, 69: 397

9 Eldridge J I, Spuckler C M. *Journal of the American Ceramic Society*[J], 2008, 91(5): 1603

10 Li C M, Luo H J, Zhao N *et al*. *Rare Metal Materials and Engineering*[J], 2025, 54(9): 2189

11 Chen Y H, Lan B, Lin Y Y *et al*. *Rare Metal Materials and Engineering*[J], 2025, 54(10): 2403

12 Song J B, Wang L S, Dong H *et al*. *Ceramics International*[J], 2023, 49(1): 1

13 Lashmi P G, Ananthapadmanabhan P V, Unnikrishnan G *et al*. *Journal of the European Ceramic Society*[J], 2020, 40(8): 2731

14 Gildersleeve E J, Vaßen R. *Journal of Thermal Spray Technology*[J], 2023, 32(4): 778

15 Liu S H, Li C X, Li L *et al*. *Surface and Coatings Technology*[J], 2018, 337: 241

16 Shi M, Xue Z J, Zhang Z *et al*. *Surface and Coatings Technology*[J], 2020, 395: 125946

17 Xiao Y, Ren E R, Hu M *et al*. *Coatings*[J], 2018, 8(9): 1099

18 Xie S M, Song C, Liu S W *et al*. *Surface and Coatings Technology*[J], 2021, 416: 127175

19 Xu Y J, Guo X J, Lin C C *et al*. *Journal of Thermal Spray Technology*[J], 2020, 29(4): 574

20 Dong S, Kong L C, Fu B G *et al*. *Ceramics International*[J], 2022, 48(24): 36441

21 Dong Y S, Yan C L, Li J *et al*. *Ceramics International*[J], 2023, 49(12): 20034

22 Kim K S, Park J M, Choi S *et al*. *Journal of Physics D: Applied Physics*[J], 2008, 41(6): 065401

23 Zhang N N, Sun F, Zhu L *et al*. *Journal of Thermal Spray Technology*[J], 2011, 20(6): 1321

24 Leins M, Kopecki J, Gaiser S *et al*. *Contributions to Plasma Physics*[J], 2014, 54(1): 14

25 Jin X, Zhao P, Zeng M *et al*. *Journal of Thermal Spray Technology*[J], 2023, 32(7): 1662

26 Li X Y, Zhou Z W, Li R Y *et al*. *Plasma Science and Technology*[J], 2023, 25(5): 055504

27 Murphy A B. *Plasma Chemistry and Plasma Processing*[J], 2023, 43(5): 1277

28 Park H, Choe W. *Current Applied Physics*[J], 2010, 10(6): 1456

29 Geng C, Zhao P, Wu M *et al*. *Ceramics International*[J], 2024, 50(1): 1360

30 Huang H J, Pan W X, Guo Z Y *et al*. *IEEE Transactions on Plasma Science*[J], 2008, 36(4): 1050

31 Takahashi H, Okamoto A, Kitajima S *et al*. *Contributions to Plasma Physics*[J], 2017, 57(8): 322

32 Hong Y, Niu J, Pan J *et al*. *Vacuum*[J], 2016, 130: 130

H_2对电弧等离子体炬制备8YSZ涂层的影响

耿传文[1]，赵 鹏[2]，苏 毅[2]，范子豪[3]，吴 曦[4]

(1. 安徽理工大学 碳中和科学与工程学院，安徽 合肥 232001)

(2. 中国科学院 等离子体物理研究所，安徽 合肥 230031)

(3. 安徽工业大学 冶金工程学院，安徽 马鞍山 243032)

(4. 石河子大学 化学化工学院，新疆 石河子 832003)

摘 要：使用8YSZ颗粒喷涂技术制备热障涂层（TBCs），通常会在等离子体炬放电气体中加入H_2。通过改变工作气体中H_2含量，研究H_2对放电产生的影响，同时结合粒子速度捕获诊断、光学发射光谱仪和有限元模拟，验证H_2含量与涂层质量之间的联系。结果表明：添加H_2会提高等离子体温度和速度，从而提高熔融8YSZ颗粒的效率和飞行速度。然而，将$H_2/(Ar+H_2)$的值提高到50%，电弧根部的不稳定性影响电弧等离子体放电，这使得保持飞行粒子的物理状态变得具有挑战性。随着H_2流速的升高，涂层质量呈现先上升后下降的趋势，最佳流速比为$H_2/(Ar+H_2)$=37.5%。该研究结果可以为等离子体制备TBCs提供理论指导。

关键词：飞行颗粒；8YSZ涂层；等离子体炬；H_2等离子体

作者简介：耿传文，男，1992年生，博士，安徽理工大学碳中和科学与工程学院，安徽 合肥 232001，E-mail：chuanwen.geng@aust.edu.cn